WUE-ITP-2002.002
DESY 01-173
HEPHY-PUB 743
ZU-TH 38/01
LC-TH-2003-031

Selectron Pair Production at e^-e^- and e^+e^- Colliders with Polarized Beams

C. Blöchinger[1], H. Fraas[1], G. Moortgat-Pick[2] and W. Porod[3,4]

[1]Institut für Theoretische Physik und Astrophysik,
Universität Würzburg, D-97074 Würzburg, Germany
[2]DESY, Deutsches Elektronen-Synchrotron, D-22603 Hamburg, Germany
[3]Inst. f. Hochenergiephysik, Öster. Akademie d. Wissenschaften,
A-1050 Vienna, Austria
[4]Inst. für Theor. Physik, Universität Zürich, CH-8057 Zürich, Switzerland

June 26, 2003

Abstract

We investigate selectron pair production and decay in e^-e^- scattering and e^+e^- annihilation with polarized beams taking into account neutralino mixing as well as ISR and beamstrahlung corrections. One of the main advantages of having both modes at disposal is their complementarity concerning the threshold behaviour of selectron pair production. In e^-e^- the cross sections at threshold for $\tilde{e}_R\tilde{e}_R$ and $\tilde{e}_L\tilde{e}_L$ rise proportional to the momentum of the selectron and in e^+e^- that for $\tilde{e}_R\tilde{e}_L$. Measurements at threshold with polarized beams can be used to determine the selectron masses $m_{\tilde{e}_{L/R}}$ precisely. Moreover we discuss how polarized electron and positron beams can be used to establish directly the weak quantum numbers of the selectrons. We also use selectron pair production to determine the gaugino mass parameter M_1. This is of particular interest for scenarios with non-universal gaugino masses at a high scale resulting in $|M_1| \gg |M_2|$ at the electroweak scale. Moreover, we consider also the case of a non-vanishing selectron mixing and demonstrate that it leads to a significant change in the phenomenology of selectrons.

1 Introduction

Supersymmetry (SUSY) is one of the most promising concepts for physics beyond the Standard Model (SM) and we expect that candidates for supersymmetric particles will first be discovered at the LHC. Due to the clear signatures linear colliders are well suited for high precision studies [1, 2, 3]. In addition to suitable cuts a simultaneous polarization of both beams is crucial for suppression of the background. One of the most important goals of a future e^+e^- or e^-e^- linear collider (LC) will be the precise determination of quantum numbers and couplings of supersymmetric particles in order to establish the supersymmetric framework. Also for some of these measurements beam polarization is indispensable [4].

Since in many cases the e^+e^- mode is favourable most of the running time will be spent for this mode. However, for some processes the e^-e^- mode is accepted to be superior, particularly for the precise measurement of the selectron masses [5, 6]. This is due to the steeper rise of the cross sections for $\tilde{e}^-_R\tilde{e}^-_R$ and $\tilde{e}^-_L\tilde{e}^-_L$ production in e^-e^- at the threshold compared to selectron production in e^+e^- annihilation [5, 6, 7]. Most of these analyses assume that the lightest neutralino is a pure B–ino so that in $\tilde{e}^-_R\tilde{e}^-_R$ production the contributions from the exchange of the other neutralinos can be neglected. In the study presented here we take into account neutralino mixing and give also results for $\tilde{e}^-_L\tilde{e}^-_L$ and $\tilde{e}^-_R\tilde{e}^-_L$ production. In the e^-e^- mode the cross sections are in general larger than in the e^+e^- mode due to the absence of destructive interferences between s–channel and t/u–channel exchange [8]. Moreover, a significantly lower background from SM and SUSY is expected in the e^-e^- mode.

In order to establish Supersymmetry it is necessary to verify experimentally the association of chiral fermions and their scalar SUSY partners. Moreover, for the identification of the supersymmetric scenario the precise determination of model parameters is necessary. In particular for the determination of the gaugino mass parameter M_1 of the MSSM and a test of gaugino mass unification divers procedures have already been discussed [5, 9]. Since the cross section for $e^-e^- \to \tilde{e}^-_R\tilde{e}^-_R$ shows a strong dependence on M_1 [5, 10] this process offers also a possibility of its measurement. The precision will, however, depend on the mixing of the neutralino states.

The main focus of this paper is on the comparison of e^-e^- scattering and e^+e^- annihilation for the production of selectron pairs. It is organised as follows. In Sect. 2 we compare in the framework of the MSSM the cross sections for the production of selectron pairs $\tilde{e}_R\tilde{e}_R$, $\tilde{e}_L\tilde{e}_L$ and $\tilde{e}_R\tilde{e}_L$ in e^+e^- annihilation and e^-e^- scattering. We take into account a general neutralino mixing and the effects of initial state radiation (ISR) as well as beamstrahlung. We emphasise the importance of beam polarization. In Sect. 3 the threshold behaviour of the cross sections for the three selectron production channels is compared for the two linear collider modes with regard to the measurement of the mass of the right and left selectron, respectively. We demonstrate in Sect. 4 the possibility to establish the partnership between chiral electrons and their scalar partners in e^+e^- annihilation with suitably polarized beams. In Sect. 5 we investigate the M_1 dependence of the production cross sections. In Sect. 6 we discuss the implications of a possible mixing between left and right selectrons. The summary is given in Sect. 7. In the Appendices we collect the formulas for the production cross sections in the e^+e^- and in the e^-e^- mode for polarized beams as well as for general selectron mixing.

2 Impact of beam polarization on selectron pair production

We compare selectron production in e^+e^- annihilation via γ– and Z^0–exchange in the s–channel and $\tilde{\chi}^0_i$–exchange ($i = 1, \ldots, 4$) in the crossed channel, and in e^-e^- scattering,

scenario	$m_{\tilde{\chi}_1^\pm}$	$m_{\tilde{\chi}_2^\pm}$	$m_{\tilde{\chi}_1^0}$	$m_{\tilde{\chi}_2^0}$	$m_{\tilde{\chi}_3^0}$	$m_{\tilde{\chi}_4^0}$
(I)	127.7	345.8	69.7	130.1	319.8	348.5
(II)	126.4	349.1	102.1	154.2	183.3	349.8

Table 1: Chargino and neutralino masses ([GeV]) for scenario (I) ($M_2 = 152$ GeV, $\mu = 316$ GeV, $\tan\beta = 3$) and scenario (II) ($M_2 = 320$ GeV, $\mu = 150$ GeV, $\tan\beta = 3$)

scenario	$\nu_e\tilde{\chi}_1^\pm$	$e^-\tilde{\chi}_1^0$	$e^-\tilde{\chi}_2^0$
(I)	0.534	0.144	0.322
(II)	0.986	0.011	0.003

Table 2: Branching ratios of $\tilde{e}_L^-$ for both scenarios (I) and (II).

where only $\tilde{\chi}_i^0$–exchange contribute. We study the different selectron final states in two MSSM scenarios. In the following we use the GUT relation $M_1 = \frac{5}{3}\tan^2\Theta_W M_2$ for the gaugino mass parameters except in Sect. 5. In the first scenario (I) we take $M_2 = 152$ GeV, $\mu = 316$ GeV and $\tan\beta = 3$. Here the LSP $\tilde{\chi}_1^0$ is bino–like and the lighter chargino $\tilde{\chi}_1^\pm$ is wino–like. In the second scenario (II) with M_2 =320 GeV, μ =150 GeV, $\tan\beta = 3$ both the LSP and the lighter chargino are higgsino–like. However, the LSP has a sizable bino–component. The neutralino masses for both scenarios are given in Table 1. For the selectron masses we take $m_{\tilde{e}_L}$ =179.3 GeV and $m_{\tilde{e}_R}$ =137.7 GeV.

The decays of the selectrons are already extensively studied [8]. The right selectron couples mainly to the bino-component of the neutralino. It decays therefore mainly in $\tilde{\chi}_i^0 e$, where i denotes the neutralino with the largest bino component. The left selectron decays preferably into the wino-like chargino and a neutrino, followed by a wino-like neutralino and an electron if all decays are kinematically allowed.

2.1 e^+e^- Annihilation

In e^+e^- annihilation $\tilde{e}_R^+\tilde{e}_R^-$ and $\tilde{e}_L^+\tilde{e}_L^-$ pairs are produced in a p–wave state with cross sections which rise at threshold as β^3, where $\beta = 2p/\sqrt{s}$ is proportional to the selectron momentum:

$$e_L^+e_R^- \rightarrow \tilde{e}_R^+\tilde{e}_R^-, \tag{1}$$
$$e_R^+e_L^- \rightarrow \tilde{e}_L^+\tilde{e}_L^-\,. \tag{2}$$

The processes are mediated by γ/Z–exchange in the s–channel and neutralino exchange in the t–channel [8]. In contrast to RR and LL selectron pairs the RL pairs are produced by electrons and positrons with the same chirality

$$e_L^+e_L^- \rightarrow \tilde{e}_R^+\tilde{e}_L^-, \tag{3}$$
$$e_R^+e_R^- \rightarrow \tilde{e}_L^+\tilde{e}_R^-\,. \tag{4}$$

They are produced in an s–wave state via t–channel exchange of neutralinos with cross sections rising at threshold proportional to β.

We show for $\sqrt{s} = 500$ GeV the dependence on beam polarization of the cross sections for the different production channels for scenario (I) in Fig. 1a, c, and e and for scenario (II) in Fig. 1b, d, and f. The effects of ISR and beamstrahlung have been included. For ISR we use the structure function prescription [11] and for beamstrahlung we generate the spectrum from the approximate integral equation given in [12]. In the white areas which corresponds to the proposed TESLA design [3] the cross sections in scenario (I) for $e^+e^- \to \tilde{e}_R^+\tilde{e}_R^-$ and $e^+e^- \to \tilde{e}_R^+\tilde{e}_L^-$ vary by about a factor 20 and that for $e^+e^- \to \tilde{e}_L^+\tilde{e}_L^-$ by about a factor 10. For right polarized electrons ($P_{e^-} = 0.8$) and left polarized positrons ($P_{e^+} = -0.6$) one obtains the highest cross section of 1340 fb for the production of $\tilde{e}_R^+\tilde{e}_R^-$ pairs. Those for the other pairs $\tilde{e}_R^+\tilde{e}_L^-$ and $\tilde{e}_L^+\tilde{e}_L^-$ lead to rates less than 30 fb. In the scenario (II) the rates for $\tilde{e}_R^+\tilde{e}_R^-$ and $\tilde{e}_L^+\tilde{e}_L^-$ are significantly smaller than in scenario (I) because in this case the interference between the s– and the t–channel is more destructive. The rates for $\tilde{e}_R^+\tilde{e}_L^-$ increase. The polarization dependence of $\sigma(e^+e^- \to \tilde{e}_L^+\tilde{e}_R^-)$ is obtained by reversing the sign of P_{e^-} and P_{e^+} in Fig. 1c and d, as a consequence of the pure t–channel exchange.

2.2 e^-e^- Scattering

Right and left selectrons are produced by right– and left–handed electrons since only t– and u–channel exchange of neutralinos contribute:

$$\begin{aligned} e_R^- e_R^- &\to \tilde{e}_R^- \tilde{e}_R^-, & (5)\\ e_L^- e_L^- &\to \tilde{e}_L^- \tilde{e}_L^-, & (6)\\ e_R^- e_L^- &\to \tilde{e}_R^- \tilde{e}_L^-. & (7) \end{aligned}$$

In contrast to e^+e^- annihilation RR and LL pairs are produced in a s–wave state with the cross sections at threshold rising as β, whereas RL pairs are produced in a p–wave state with a β^3 behaviour of the threshold cross section.

The polarization dependence of the cross sections is depicted in Fig. 2a, c, e for scenario (I) and in Fig. 2b, d, f for scenario (II) for $\sqrt{s} = 500$ GeV. Here we have taken into account the effects of ISR and beamstrahlung. For ISR we use the structure function prescription [11] and for beamstrahlung we use the energy distribution given by Eq. (6) in [12] evaluated with the approximation P2. For the luminosity enhancement parameter we use the analytic approximation given by Eq. (14) in [13].

Quite generally the cross sections are larger than for selectron production by e^+e^- annihilation. For the highest polarization in the TESLA design, $P_{e_{1,2}} = \pm 0.8$ for the electron beams, one obtains for the production of $\tilde{e}_R^-\tilde{e}_R^-$ and $\tilde{e}_L^-\tilde{e}_L^-$ cross sections of about 2.5 pb for $P_{e_{1,2}} = 0.8$ and $P_{e_{1,2}} = -0.8$, respectively. For the production of left–right selectron pairs a maximal cross section of 360 fb in scenario (I) and 400 fb in scenario (II) is reached for $P_{e_1} = 0.8$, $P_{e_2} = -0.8$.

According to Eqs. (5) – (7) the cross section for RR (LL) pairs vanishes if one of the electron beams is completely left–handed (right–handed) polarized and that for RL pairs vanishes if both beams are completely polarized with the same sign.

3 Threshold behaviour

The precision on the determination of the masses of $\tilde{e}_R$ and $\tilde{e}_L$ in e^+e^- annihilation and e^-e^- scattering, respectively, depends on both the threshold behaviour of the cross sections for the different production channels and on a suitable choice of beam polarizations. As we are mainly interested in the comparison of the collider modes we take into account statistical

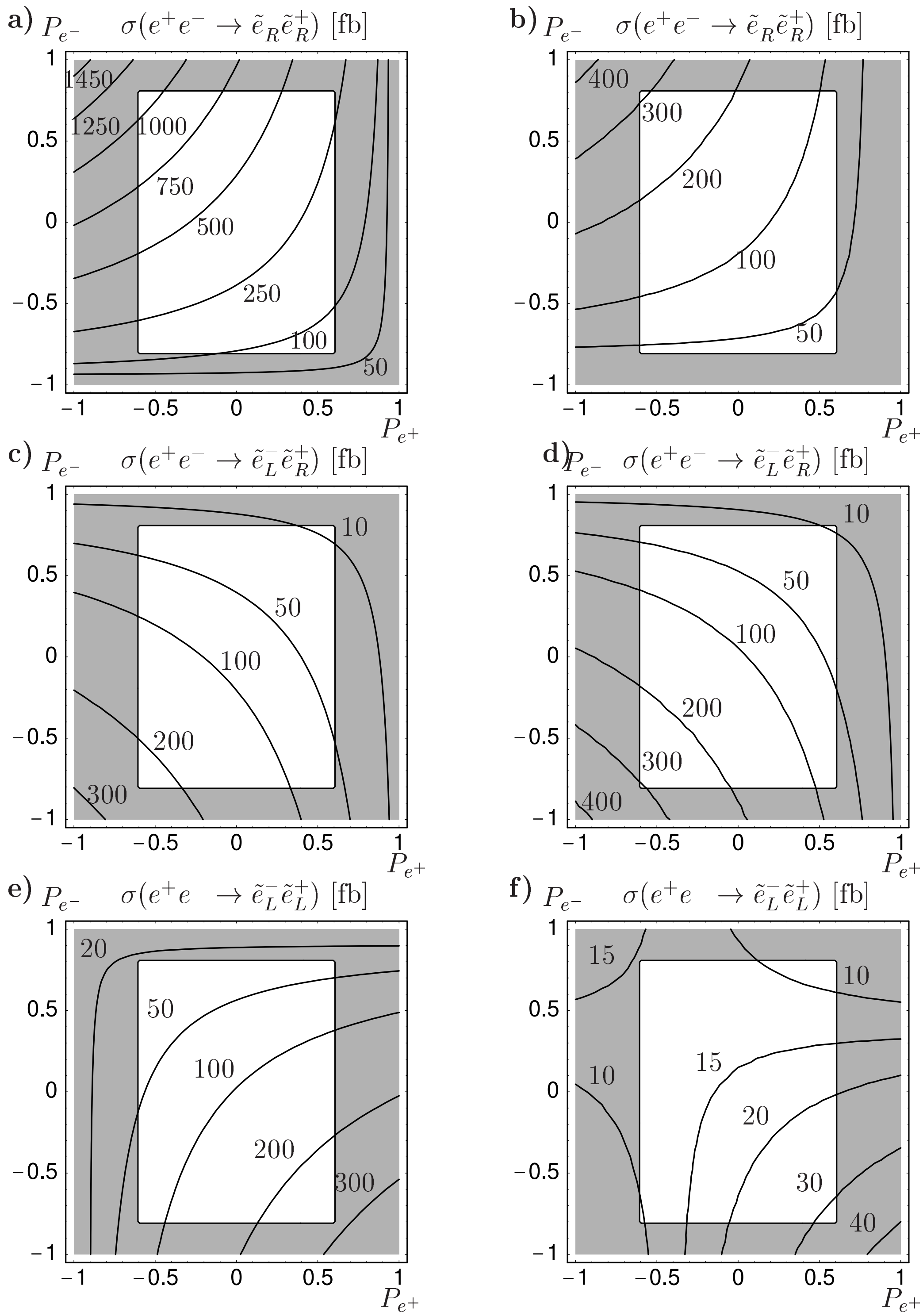

Figure 1: Contour lines for the cross sections in fb for **a)** and **b)** $\sigma(e^+e^- \to \tilde{e}_R^- \tilde{e}_R^+)$, **c)** and **d)** $\sigma(e^+e^- \to \tilde{e}_L^- \tilde{e}_R^+)$, **e)** and **f)** $\sigma(e^+e^- \to \tilde{e}_L^- \tilde{e}_L^+)$ as a function of electron polarization P_{e^-} and positron polarization P_{e^+} for $\sqrt{s} = 500$ GeV, $m_{\tilde{e}_R} = 137.7$ GeV, $m_{\tilde{e}_L} = 179.3$ GeV, $\tan\beta = 3$; in **a)**, **c)** and **e)** $M_2 = 152$ GeV, $\mu = 316$ GeV and in **b)**, **d)** and **f)** $M_2 = 320$ GeV, $\mu = 150$ GeV. ISR corrections and beamstrahlung are included. The white area shows the region which can be realized within the TESLA design with $|P_{e^-}| = 0.8$, $|P_{e^+}| = 0.6$.

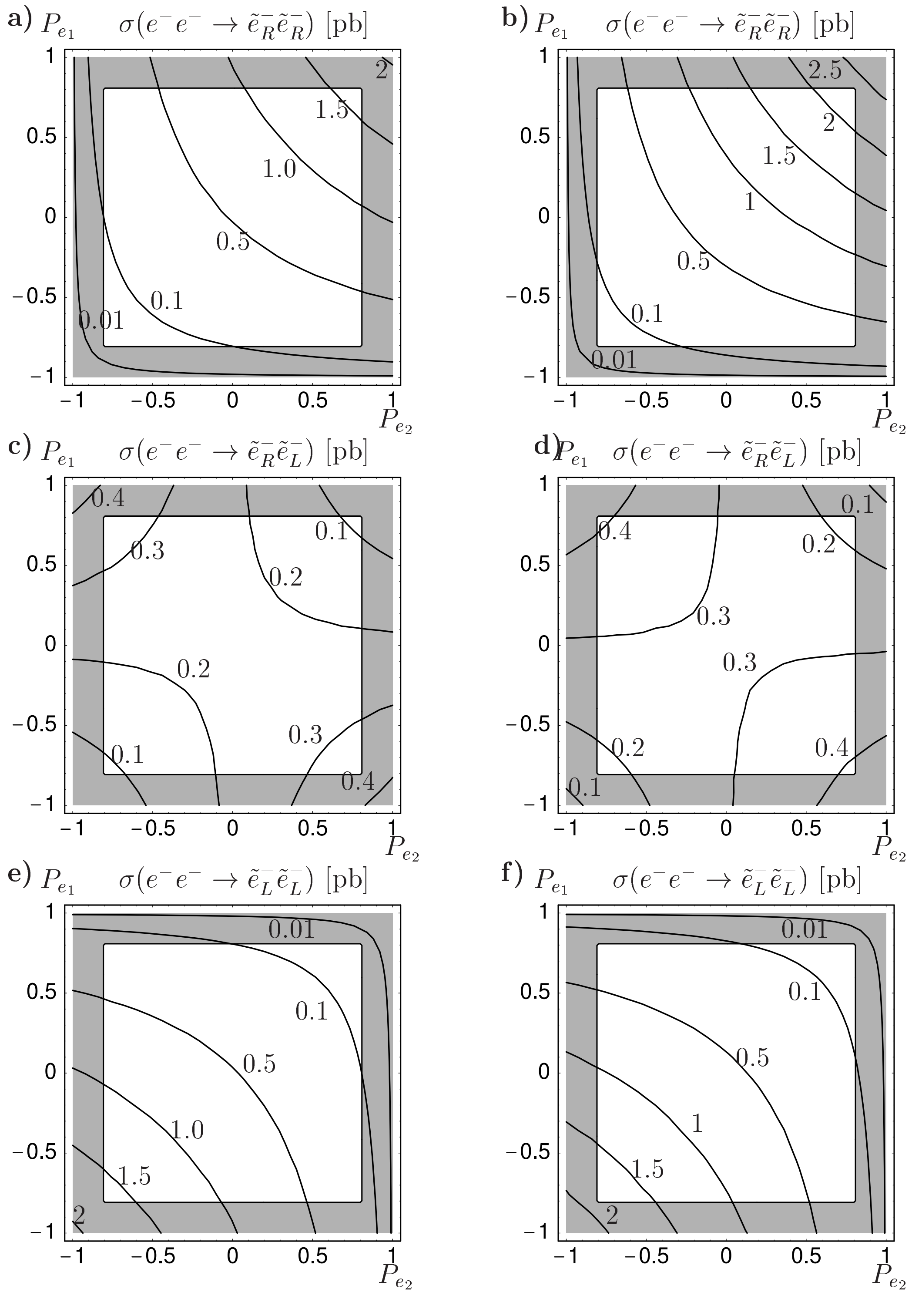

Figure 2: Contour lines for the cross sections in pb for **a)** and **b)** $\sigma(e^-e^- \to \tilde{e}_R^-\tilde{e}_R^-)$, **c)** and **d)** $\sigma(e^-e^- \to \tilde{e}_R^-\tilde{e}_L^-)$, **e)** and **f)** $\sigma(e^-e^- \to \tilde{e}_L^-\tilde{e}_L^-)$ as a function of electron polarizations $P_{e_{1/2}}$ for $\sqrt{s} = 500$ GeV, $m_{\tilde{e}_R} = 137.7$ GeV, $m_{\tilde{e}_L} = 179.3$ GeV, $\tan\beta = 3$; in **a)**, **c)** and **e)** $M_2 = 152$ GeV, $\mu = 316$ GeV and in **b)**, **d)** and **f)** $M_2 = 320$ GeV, $\mu = 150$ GeV. ISR corrections and beamstrahlung are included. The white area shows the region which can be realized within the TESLA design with $|P_{e_{1,2}}| = 0.8$.

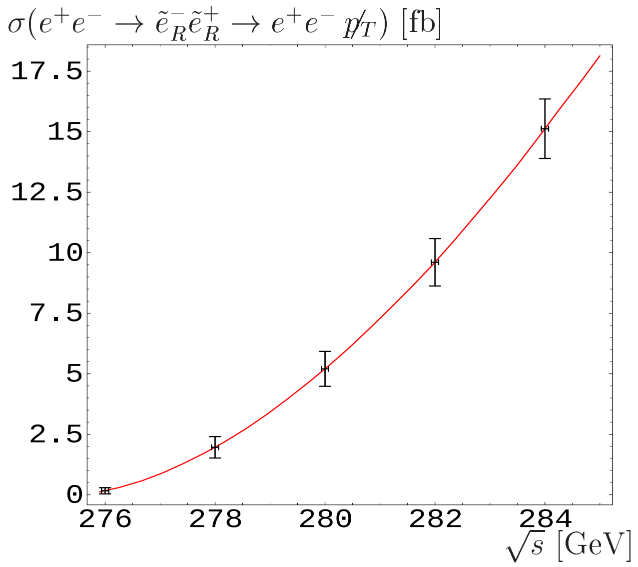

Figure 3: Threshold behaviour of the process $e^+e^- \to \tilde{e}_R^-\tilde{e}_R^+ \to e^+e^- \not{p}_T$ for $P_{e^-} = +0.8$ and $P_{e^+} = -0.6$, $M_2 = 152$ GeV, $\mu = 316$ GeV and $\tan\beta = 3$. ISR corrections and beamstrahlung are included. The error bars show the statistical error for $\mathcal{L} = 10$ fb^{-1}.

errors only disregarding effects of the finite widths of the selectrons, which will be studied in future investigations [14], and of beam energy spread which would need Monte Carlo simulations. The comparison is done for scenario (I) of Table 1. We comment on scenario (II) at the end of this section. The determination of selectron masses in the continuum is discussed in [15].

3.1 Measurement of $m_{\tilde{e}_R}$

In scenario (I) the right selectron decays nearly always into an electron and the LSP. Therefore, the signature of $\tilde{e}_R$ pair production in e^+e^- annihilation (e^-e^- scattering) is an e^+e^- (e^-e^-) pair and missing energy. In the following we assume an effective luminosity of 10 fb^{-1} in case of e^+e^- and an effective luminosity of 1 fb^{-1} in case of e^-e^- at each scanning step.

3.1.1 e^+e^- Annihilation

The favourable polarization is $P_{e^-} = +0.8$ and $P_{e^+} = -0.6$. In this case one obtains both the highest cross sections for $e^+e^- \to \tilde{e}_R^+\tilde{e}_R^-$ and maximal suppression of the SM background from W and Z^0 pair production and from single W production. Also for this configuration of beam polarizations the SUSY background processes $e^+e^- \to \tilde{\chi}_1^0\tilde{\chi}_2^0 \to \tilde{\chi}_1^0\tilde{\chi}_1^0 e^+e^-$ and $e^+e^- \to \tilde{\chi}_2^0\tilde{\chi}_2^0 \to \tilde{\chi}_1^0\tilde{\chi}_1^0 \nu_e\bar{\nu}_e e^+e^-$ are reduced.

Fig. 3 shows for these polarizations the cross sections near threshold for $e^+e^- \to \tilde{e}_R^+\tilde{e}_R^- \to e^+e^-\tilde{\chi}_1^0\tilde{\chi}_1^0$ for $m_{\tilde{e}_R} = 137.7$ GeV, and the 1σ error bars for an effective luminosity of $\mathcal{L} = 10$fb^{-1} for each point. The horizontal error bars indicate the expected errors on the selectron mass. Provided the neutralino mass parameters are precisely known the measurement of the cross section at five points results in an error of $\Delta m_{\tilde{e}_R} = 65$ MeV. Since the statistical error is comparable to the influence of the finite width of the selectrons and of the Coulomb rescattering [16, 14] these effects have to be taken into account for a precise determination of

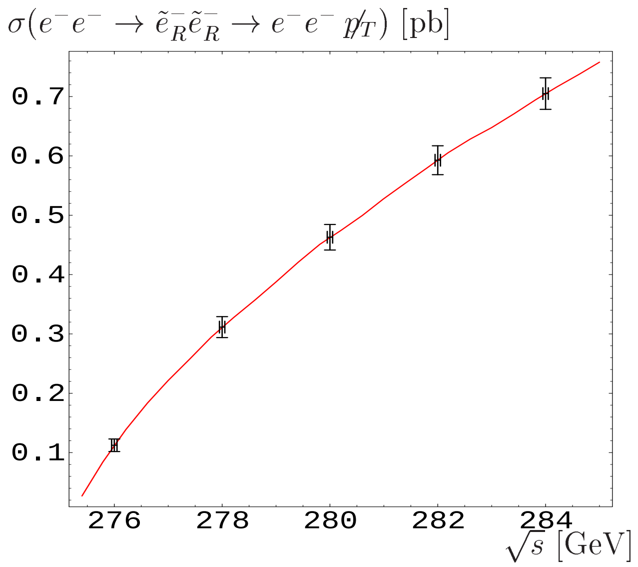

Figure 4: Threshold behaviour of the process $e^-e^- \to \tilde{e}_R^-\tilde{e}_R^- \to e^-e^- \not{p}_T$ for polarizations: $P_{e_1} = 0.8$ and $P_{e_2} = 0.8$. ISR corrections and beamstrahlung are included. The error bars show the statistical error for $\mathcal{L} = 1$ fb^{-1}.

$m_{\tilde{e}_R}$. Note that this precise determination allows a precise determination of the underlying SUSY parameters. This in turn allows for a precise determination of parameters at high energy scales [17].

3.1.2 e^-e^- Scattering

In e^-e^- scattering the favourable beam polarization leading to the largest cross sections is $P_{e_1} = P_{e_2} = 0.8$. In this case the most important backgrounds $e^-e^- \to W^-e^-\nu_e$, $W^-W^-\nu_e\nu_e$ from SM processes and $e^-e^- \to \tilde{\chi}_1^-\tilde{\chi}_1^0 e^-\nu_e$ from SUSY are suppressed. For this purpose simultaneous polarization of both beams is important.

In spite of the lower luminosity in e^-e^- scattering compared to e^+e^- annihilation the steep β rise of the cross section at threshold allows the determination of the mass of $\tilde{e}_R$ with a slightly higher precision, $m_{\tilde{e}_R} = 137.7 \pm 0.05$ GeV, which is demonstrated in Fig. 4 for a beam polarizations $P_{e_1} = P_{e_2} = 0.8$. The error bars correspond to an effective luminosity $\mathcal{L} = 1$ fb^{-1} for each point. The statistical error is as in the case of an e^+e^- collider comparable to the influence of the finite width of the selectrons and of the Coulomb rescattering which have to be taken into account for a precise determination of $m_{\tilde{e}_R}$ [16, 14].

3.2 Measurement of $m_{\tilde{e}_L}$

3.2.1 e^+e^- Annihilation

In principle the left selectron mass can be determined by a threshold scan of either $\tilde{e}_R^{\pm}\tilde{e}_L^{\mp}$ production or $\tilde{e}_L^+\tilde{e}_L^-$ production. If $m_{\tilde{e}_R}$ is already known the production of a pair of left–right selectrons is more suitable due to the threshold behaviour with the steeper β rise. For $e^+e^- \to \tilde{e}_R^+\tilde{e}_L^-$ ($\tilde{e}_L^+\tilde{e}_R^-$) the polarization $P_{e^-} = -0.8$, $P_{e^+} = -0.6$ ($P_{e^-} = 0.8$, $P_{e^+} = 0.6$) leads to the largest cross sections.

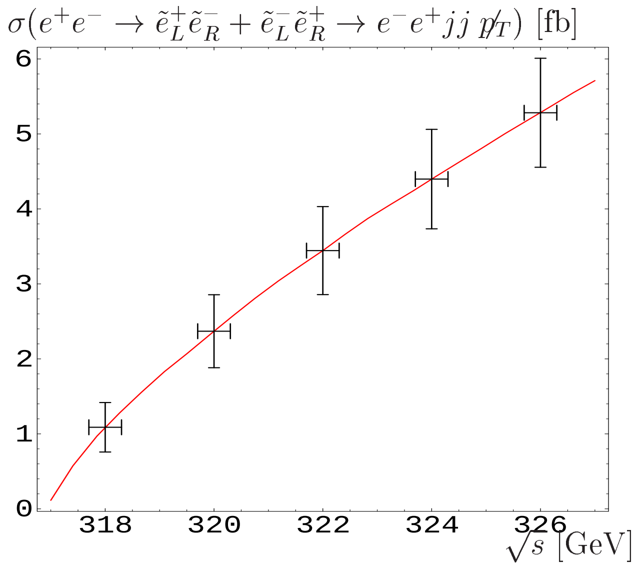

Figure 5: Threshold behaviour of the processes $e^+e^- \to \tilde{e}_L^+\tilde{e}_R^- + \tilde{e}_L^-\tilde{e}_R^+ \to e^-e^+jj\ \not{p}_T$ for $P_{e^-} = 0.8$ and $P_{e^+} = 0.6$, $M_2 = 152$ GeV, $\mu = 316$ GeV and $\tan\beta = 3$. ISR corrections and beamstrahlung are included. The error bars show the statistical error for $\mathcal{L} = 10$ fb^{-1}.

In our scenario $\tilde{e}_R^-$ decays into an electron and the LSP, whereas for the left selectron the following decays are allowed: $\tilde{e}_L^- \to e\tilde{\chi}_1^0$, $\tilde{e}_L^- \to e\tilde{\chi}_2^0$ and $\tilde{e}_L^- \to \nu_e\tilde{\chi}_1^-$. The decays of the chargino $\tilde{\chi}_1^-$ as well as the neutralino $\tilde{\chi}_2^0$ decay lead to four-particle final states.

The final state $e^+e^-\not{p}_T$ is not suitable for the identification of the $\tilde{e}_R\tilde{e}_L$ pair since the background from $\tilde{e}_R^+\tilde{e}_R^-$ production is significantly larger than the signal $e^+e^- \to \tilde{e}_R^+\tilde{e}_L^- + \tilde{e}_R^-\tilde{e}_L^+ \to e^+e^-\tilde{\chi}_1^0\tilde{\chi}_1^0 + e^+e^-\tilde{\chi}_1^0\tilde{\chi}_1^0\nu\nu$. Even for $P_{e^-} = -0.8$, $P_{e^+} = -0.6$, where the signal is largest, the ratio of the cross sections RR:RL is 5:1. The final state should contain an e^+e^- pair for the identification of the flavour of the produced sleptons. Therefore, we consider the decay $\tilde{e}_L^\pm \to e^\pm\tilde{\chi}_2^0 \to e^\pm jj\not{p}_T$, where j denotes a jet and we assume a $BR(\tilde{\chi}_2^0 \to jj\tilde{\chi}_1^0) = 0.35$. The main SM background stems from triple gauge boson production W^+W^-Z, $W^+W^-\gamma^*$ and ZZZ. The cross section for these processes leading to the final state $e^+e^-jj\not{p}_T$ is below 1 fb [18]. It is further suppressed by our choice of beam polarization. The main SUSY background from $e^+e^- \to \tilde{\chi}_2^0\tilde{\chi}_2^0 \to e^+e^-jj\not{p}_T$ has in general a different event topology compared to our signal and can also be suppressed by an appropriate choice of beam polarization.

We show in Fig. 5 the threshold for $e^+e^- \to \tilde{e}_R^-\tilde{e}_L^+ + \tilde{e}_R^+\tilde{e}_L^- \to e^+e^-jj\not{p}_T$ for scenario (I) and $P_{e^-} = 0.8$, $P_{e^+} = 0.6$ so that the signal is maximal and the SUSY background is minimal. Assuming 5 data points with an integrated luminosity of 10 fb^{-1} for each we find a statistical error of $\Delta m_{\tilde{e}_L^\pm} = 300$ MeV.

The cross section for $e^+e^- \to \tilde{e}_L^-\tilde{e}_L^+ \to e^+e^-jjjj\not{p}_T$ is below 0.2 fb near threshold. This small cross section is caused by the β^3 dependence at threshold and by the small branching ratio of $\tilde{e}_L$ into $ejj\not{p}_T$ in our scenario. This implies a rather large statistical error resulting in $\Delta m_{\tilde{e}_L^\pm} = 1.2$ GeV which is a factor 4 worse compared to the measurement at the $\tilde{e}_L^\pm\tilde{e}_R^\mp$ threshold.

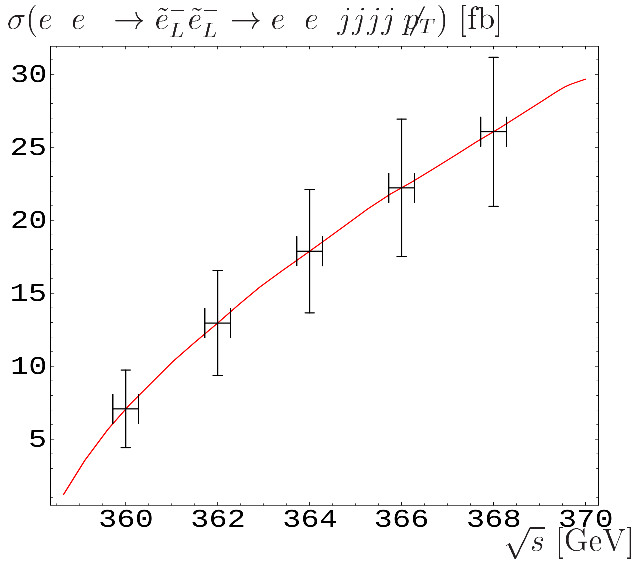

Figure 6: Threshold behaviour of the process in $e^-e^- \to \tilde{e}_L^-\tilde{e}_L^- \to e^-e^-jjjj\not{p}_T$ for $P_{e_1} = -0.8$ and $P_{e_2} = -0.8$. ISR corrections and beamstrahlung are included. The error bars show the statistical error for $\mathcal{L} = 1$ fb^{-1}.

3.2.2 e^-e^- Scattering

The process $e^-e^- \to \tilde{e}_L^-\tilde{e}_L^- \to e^-e^-jjjj\not{p}_T$ leads to larger cross sections compared the corresponding process in e^-e^+ annihilation as can be seen in Fig. 6. The cross section at threshold for polarizations $P_{e_1} = -0.8$ and $P_{e_2} = -0.8$ rises much steeper and the mass resolution therefore is much better than in e^+e^- annihilation. With the effective luminosity $\mathcal{L} = 1$ fb^{-1} the left selectron mass $m_{\tilde{e}_L} = 179.3 \pm 0.28$ GeV can be determined precisely. For completeness we note that one obtains in the process $e^-e^- \to \tilde{e}_R^-\tilde{e}_L^- \to e^-e^-jj\ \not{p}_T$ a mass resolution of $m_{\tilde{e}_L} = 179.3 \pm 1.1$ GeV.

3.3 Comments on scenario II

The precision for measuring the masses in e^+e^- annihilation as well as in e^-e^- scattering depends on the scenario. Since the rate for $e^+e^- \to \tilde{e}_R^+\tilde{e}_R^-$ is about a factor four smaller in scenario (II) the accuracy for $\Delta m_{\tilde{e}_R}$ decreases by about an order of magnitude. In case of e^-e^- scattering a similar precision is expected for both scenarios. The rates for the mixed pair $\tilde{e}_R^\pm\tilde{e}_L^-$ are nearly the same as in scenario (I). However, the branching ratio for $\tilde{e}_L \to e\tilde{\chi}_2^0$ is two orders of magnitude smaller, see Table 2. Therefore, any conclusions without a detailed Monte Carlo study, which is beyond the scope of this paper, are very difficult.

4 The weak quantum numbers of the selectrons

Supersymmetry associates to the two chirality states e_L^-, e_R^- of the electrons left and right scalar partners $\tilde{e}_L^-$, $\tilde{e}_R^-$. In order to test the concept of supersymmetry it is important to test the weak quantum numbers R, L of the selectrons produced in e^+e^- annihilation. For these tests an e^+e^- collider is better suited than an e^-e^- collider because in the latter one only the negative charged selectrons can be probed. Note, however, that due to CPT the

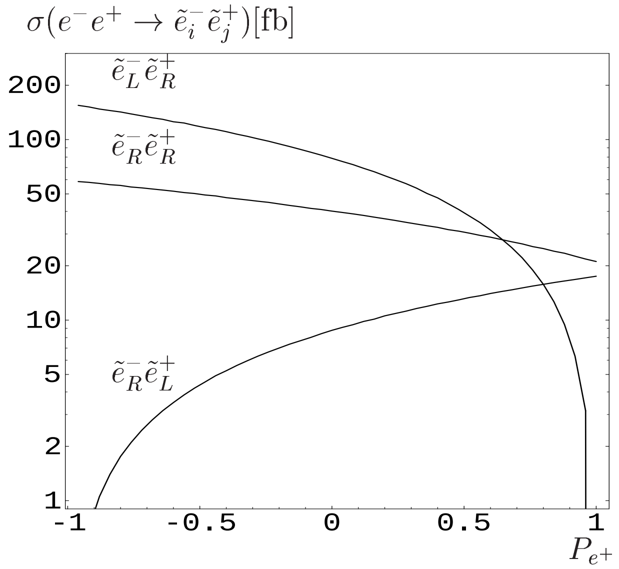

Figure 7: Production cross sections as a function of P_{e^+} for $\sqrt{s} = 350$ GeV, $P_{e^-} = -0.8$, $m_{\tilde{e}_R} = 137.7$ GeV, $m_{\tilde{e}_L} = 179.3$ GeV, $M_2 = 156$ GeV, $\mu = 316$ GeV and $\tan\beta = 3$. ISR corrections and beamstrahlung are included.

antiparticles $\tilde{e}_L^+$ and $\tilde{e}_R^+$ are the scalar partners of e_R^+ and e_L^+.

Due to the small electron mass one expects no mixing of the electroweak eigenstates $\tilde{e}_L$ and $\tilde{e}_R$. The possibility of a non–vanishing selectron mixing will be discussed in Sect. 6. Only at the $e\tilde{e}\tilde{\chi}_i^0$ vertex the chiral quantum number L, R of the electron is uniquely related to its scalar partner. These vertices appear only in the t–channel but not in the s–channel. In order to separate these channels the use of both beam polarizations is absolutely needed. In particular for electrons and positrons with the same helicity (chirality) only t–channel exchange of neutralinos contribute so that in the processes $e_L^+e_L^- \to \tilde{e}_R^+\tilde{e}_L^-$ and $e_R^+e_R^- \to \tilde{e}_L^+\tilde{e}_R^-$ they are directly coupled to their scalar partners. Therefore, the R, L quantum number are correlated to the charge of the produced selectrons. In case the electron and positron have different helicities, RR or LL pairs are produced in the t–channel, $e_L^+e_R^- \to \tilde{e}_R^+\tilde{e}_R^-$ and $e_R^+e_L^- \to \tilde{e}_L^+\tilde{e}_L^-$. However, in this configuration one obtains also both pairs RR and LL from the s–channel exchange.

For the TESLA design [3] a maximal electron (positron) polarization of $|P_{e^-}| = 0.8$ ($|P_{e^+}| = 0.6$) is proposed. Therefore we study the extent to which the test of the L, R quantum numbers is possible with partially polarized beams. In Fig. 7 we show the cross sections for $e^+e^- \to \tilde{e}_{L,R}^+\tilde{e}_{L,R}^-$ for $P_{e^-} = -0.8$ as a function of the positron polarization at $\sqrt{s} = 350$ GeV. The SUSY parameters are specified as in scenario (I). For positron polarization $P_{e^+} \lesssim 0.5$ the production cross section for $\tilde{e}_L^-\tilde{e}_R^+$ is the largest one. We give in Table 3 the production cross section for different centre of mass energies for $P_{e^-} = -0.8$ and $P_{e^+} = -0.6$. The ratio $r = \sigma(e^+e^- \to \tilde{e}_L^-\tilde{e}_R^+)/[\sigma(e^+e^- \to \tilde{e}_R^-\tilde{e}_R^+) + \sigma(e^+e^- \to \tilde{e}_R^-\tilde{e}_L^+) + \sigma(e^+e^- \to \tilde{e}_L^-\tilde{e}_L^+)]$ is larger for $\sqrt{s} = 350$ GeV ($r \simeq 2.4$) than for $\sqrt{s} = 500$ GeV ($r \simeq 1.2$). The decrease is due to kinematical effects. This ratio becomes larger with increasing electron and positron polarization: It would be 7.3 if one could polarize both beams with 90%. We want to stress again that for this investigation polarized positrons are essential in order to suppress the s–channel contribution.

For $e_R^+e_R^-$ it would be in principle possible to separate the pair $\tilde{e}_L^+\tilde{e}_R^-$. In case of $P_{e^-} = 0.8$,

$\sigma(\tilde{e}^+\tilde{e}^-)$ [fb]	$\sqrt{s}$ [GeV] 350	400	450	500
$\tilde{e}_L^+\tilde{e}_L^-$	0	14	43	72
$\tilde{e}_R^+\tilde{e}_R^-$	52	88	114	130
$\tilde{e}_R^+\tilde{e}_L^-$	125	205	234	239
$\tilde{e}_L^+\tilde{e}_R^-$	3.5	5.7	6.5	6.6

Table 3: Cross sections $\sigma(e^+e^- \to \tilde{e}^+_{L,R}\tilde{e}^-_{L,R})$ [fb] for $P_{e^-} = -0.8$ and $P_{e^+} = -0.6$ and different $\sqrt{s}$. ISR and beamstrahlung are included. The SUSY parameters are chosen as in the reference scenario (I).

$P_{e^+} = 0.6$ the cross section for $e^+e^- \to \tilde{e}_R^-\tilde{e}_R^+$ is larger than for $P_{e^-} = -0.8$, $P_{e^+} = -0.6$ implying a smaller ratio $\sigma(e^+e^- \to \tilde{e}_R^-\tilde{e}_L^+)/(\sigma(e^+e^- \to \tilde{e}_R^-\tilde{e}_R^+) + \sigma(e^+e^- \to \tilde{e}_L^-\tilde{e}_R^+) + \sigma(e^+e^- \to \tilde{e}_L^-\tilde{e}_L^+)) \simeq 1.13$ for $\sqrt{s} = 350$ GeV. Thus, the precision of the determination of the weak Quantum numbers is in this case significantly worse compared the case $\tilde{e}_R^+\tilde{e}_L^-$ discussed above.

5 M_1 Dependence

The cross sections for production of selectron pairs in e^+e^- annihilation and in e^-e^- scattering show a significant dependence on the gaugino mass parameter M_1 [10]. In the following we show that the measurement of the cross sections for production and subsequent leptonic decay of the selectrons with polarized beams is useful for the determination of M_1.

We display therefore in Fig. 8 the content $|N_{ij}|^2$ of the neutralino mass eigenstates $\tilde{\chi}_i^0$ in the basis $\tilde{B}$, $\tilde{W}_3$, $\tilde{H}_d^0$ and $\tilde{H}_u^0$ [19] as a function of M_1 fixing the other parameters as in scenario (I). For $|M_1| \lesssim 150$ GeV the lightest neutralino is bino-like, whereas for $|M_1| \gtrsim 150$ GeV it is mainly wino-like. For $|M_1| \lesssim 150$ GeV the second lightest neutralino is a wino whereas in the region 150 GeV $\lesssim |M_1| \lesssim 400$ GeV it is mainly a bino and for larger values it is higgsino-like. The neutralino $\tilde{\chi}_3^0$ is always higgsino like and the heaviest is higgsino-like for $|M_1| \lesssim 350$ GeV and bino-like for larger values of $|M_1|$. For $M_1 \lesssim -200$ GeV $\tilde{\chi}_1^\pm$ becomes lighter than $\tilde{\chi}_1^0$ and is thus theoretically excluded.

Let us now briefly discuss the M_1 dependence of the selectron decays. The right selectron decays mainly into the kinematically accessible neutralino with the largest bino-component. For the chosen parameters the preferred decay is that into the lightest neutralino and an electron. For the left selectron more channels are open with the BR's displayed in Fig. 9. It decays mainly into a chargino and a neutrino. The second important decay mode is into that kinematically accessible neutralino with the largest wino-content.

In the following we study for $\sqrt{s} = 500$ GeV the M_1 dependence of the total cross section $\sigma(e^+e^- \to \sum_{ij} \tilde{e}_i^+\tilde{e}_j^-)$ $(i,j = R, L)$ and the cross section $\sigma(e^+e^- \to \sum_{i,j} \tilde{e}_i^+\tilde{e}_j^- \to e^+e^-\not{p}_T)$. Since the right selectron decays mainly into the kinematically accessible neutralino with the largest bino–component, the direct decay $\tilde{e}_R^\pm \to e^\pm\tilde{\chi}_1^0$ dominates clearly for the chosen parameters. In our scenario the most important decay mode of $\tilde{e}_L^\pm$ is that via the lighter chargino $e_L^\pm \to \tilde{\chi}_1^\pm\nu_e \to e^\pm\tilde{\chi}_1^0 2\nu_e$. The second important decay mode is that via the kinematically accessible neutralino with the largest wino–component. For large $|M_1|$ values

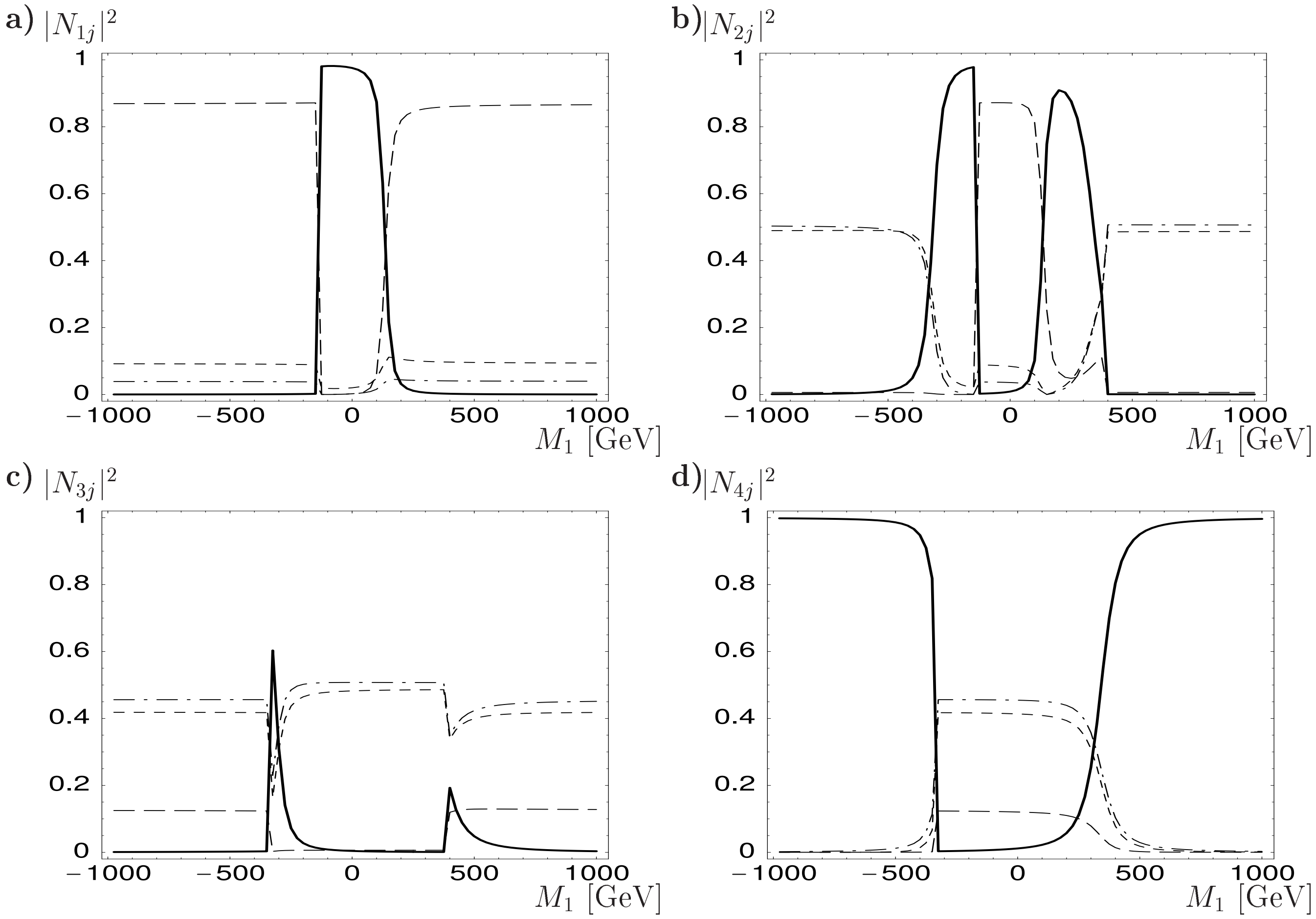

Figure 8: a) $|N_{1j}|^2$, b) $|N_{2j}|^2$, c) $|N_{3j}|^2$, and d) $|N_{4j}|^2$ as a function of M_1 for $M_2 = 152$ GeV, $\mu = 316$ GeV and $\tan\beta = 3$. The graphs correspond to the following components: full line $\tilde{B}$, long dashed line $\tilde{W}_3$, dashed line $\tilde{H}^0_d$ and long short dashed line $\tilde{H}^0_u$.

this is the direct decay $\tilde{e}^\pm_L \to \tilde{\chi}^0_1 e^\pm$ into an electron and the LSP, whereas for smaller values of M_1 this decay competes with the cascade decay $\tilde{e}^\pm \to \tilde{\chi}^0_2 e^\pm \to e^\pm \tilde{\chi}^0_1 \nu\bar{\nu}$. The branching ratios depend also on the squark sector. For a squark mass of 440 GeV one obtains in our scenario (I) a branching ratio $BR(\tilde{e}^\pm_L \to e^\pm \tilde{\chi}^0_1 2\nu) = 0.14$. We neglect in the following discussion its M_1–dependence because the variation of the chargino/neutralino branching ratios due to M_1 can be compensated by a change in the squark and/or Higgs sector. In Fig. 10 we show the M_1 dependence of **a)** the cross section for selectron production summed over all final states and **b)** the cross section for the decay leptons. The influence of ISR and beamstrahlung is different for the divers selectron pairs due to different kinematics. In case of $\tilde{e}_L\tilde{e}_L$ the cross section is decreased compared to the tree–level value whereas for the other selectron final state it is increased for $\sqrt{s} = 500$ GeV. For larger values of $\sqrt{s}$ also the $\tilde{e}_L\tilde{e}_L$ cross section increases compared to the tree-level. The M_1 dependence of the cross sections for the different selectron final states remains, however, unchanged. Since the ratios of production cross sections for the different selectron pairs depends on the beam polarization the influence of ISR and beamstrahlung modifies this polarization effect.

The M_1 dependence of both the cross section for selectron production, Fig. 10a, and for the decay electrons, Fig. 10b, depends on the beam polarization and is strongest for

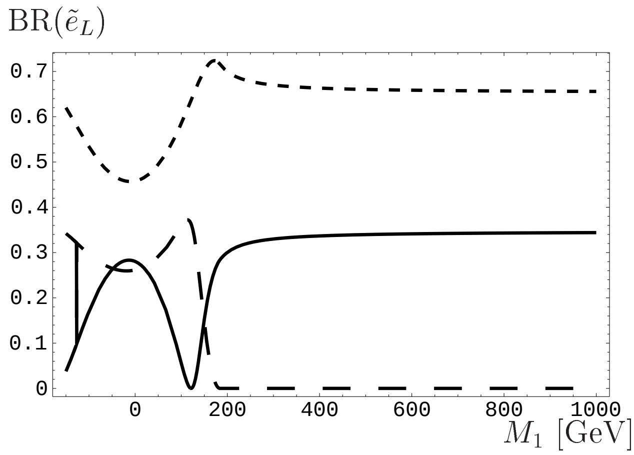

Figure 9: Branching ratios of $\tilde{e}_L$ as a function of M_1 for $m_{\tilde{e}_L} = 179.3$ GeV, $M_2 = 152$ GeV , $\mu = 316$ GeV and $\tan\beta = 3$. The graphs correspond to: full line $BR(\tilde{e}_L \to \tilde{\chi}^0_1 e^{\pm})$, long dashed line $BR(\tilde{e}_L \to \tilde{\chi}^0_2 e^{\pm})$ and dashed line $BR(\tilde{e}_L \to \tilde{\chi}^{\mp}_1 \nu_e)$.

$P_{e^-} = +0.8$, $P_{e^+} = -0.6$. In this case mainly $\tilde{e}^+_R \tilde{e}^-_R$ pairs are produced, cf. Fig. 10, which couple only to the bino component of the exchanged neutralinos. Since with increasing $|M_1|$ also the mass of the bino–like neutralino increases, the cross section decreases up to $|M_1| \sim 400$ GeV. The reason for the increase of the cross section for $|M_1| \geq 400$ GeV is the weaker M_1 dependence of the contribution from t–channel exchange compared to that of the destructive interference between s– and t–channel. The kink near $M_1 = 150$ GeV in the cross section for the decay electrons, Fig. 10b, is due to the change of the mixing character of the neutralinos, cf. Fig. 8, which leads to a strong M_1 dependence of the branching ratios shown in Fig. 9.

In case of e^-e^- the polarization dependence of the cross sections is more pronounced for large values of $|M_1|$ than in case of e^+e^- as can be seen in Fig. 11. This is due to the fact that the s-channel and therefore the destructive interference is absent. Also the cross sections are significantly larger for large $|M_1|$ in case of of e^-e^- compared to e^+e^- for the same reason. It is obvious from Figs. 10 and 11 that measuring the selectron production cross section using various combinations of electron/positron polarization is a useful tool to cross check the determination of M_1 from other measurements [20] if not providing the first measurement by itself. This might be the case if there are additional neutralinos, as e.g. in extended supersymmetric models [21] or if R-parity is broken spontaneously [22] with a right-handed scale in the 100 GeV range. In these models are more than four neutralinos and thus the observation of four neutralinos does not imply that one has found a bino-like neutralino. Moreover, different polarization configurations, in particular in case of e^-e^-, are an useful tool to determine the relative phase between M_1 and M_2. Most clearly this can be seen in Fig. 11a for the configurations $P_{e_1} = -0.8$, $P_{e_2} = -0.8$ (dashed line) and $P_{e_1} = 0.8$, $P_{e_2} = 0.8$ (long dashed line).

6 Non-vanishing selectron mixing

In this section we study consequences of a non-vanishing selectron mixing, which although theoretically disfavoured cannot be excluded. This can be seen by inspecting the mass

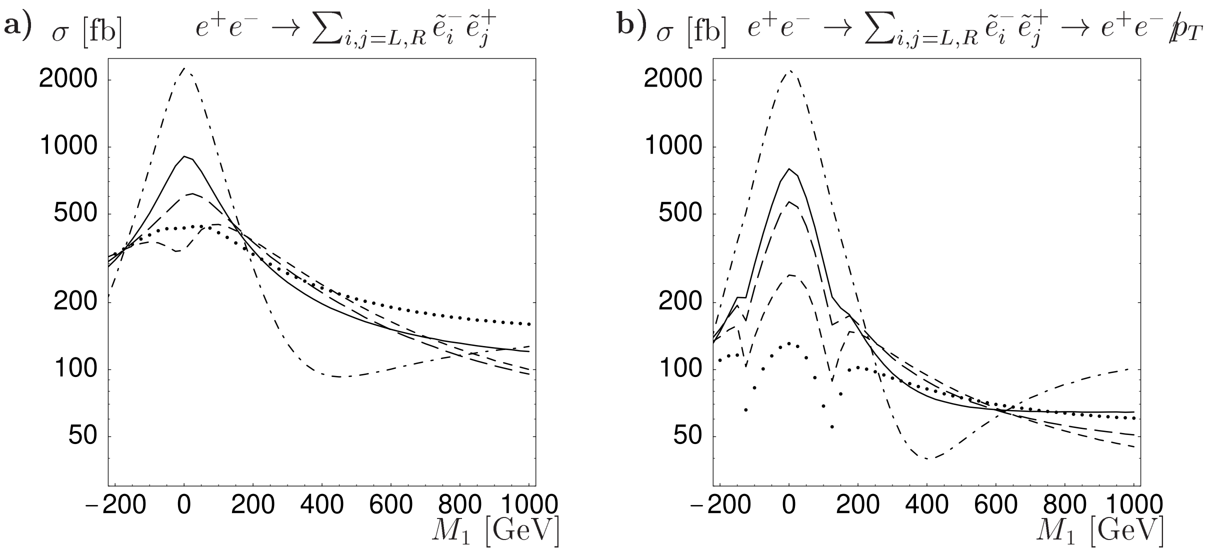

Figure 10: Cross sections for the processes $\sigma(e^+e^- \to \sum_{i,j=L,R} \tilde{e}_i^- \tilde{e}_j^+)$ (**a**) and $\sigma(e^+e^- \to \sum_{i,j=L,R} \tilde{e}_i^- \tilde{e}_j^+ \to e^+e^- \not{p}_T)$ (**b**) as a function of M_1 for various polarizations. The effects of ISR- and beamstrahlung corrections are included. The graphs correspond to the following set of polarizations: full line $P_{e^-} = 0$, $P_{e^+} = 0$, dashed line $P_{e^-} = -0.8$, $P_{e^+} = -0.6$, dashed-dotted line $P_{e^-} = 0.8$, $P_{e^+} = -0.6$, dotted line $P_{e^-} = -0.8$, $P_{e^+} = 0.6$, and long dashed line $P_{e^-} = 0.8$, $P_{e^+} = 0.6$.

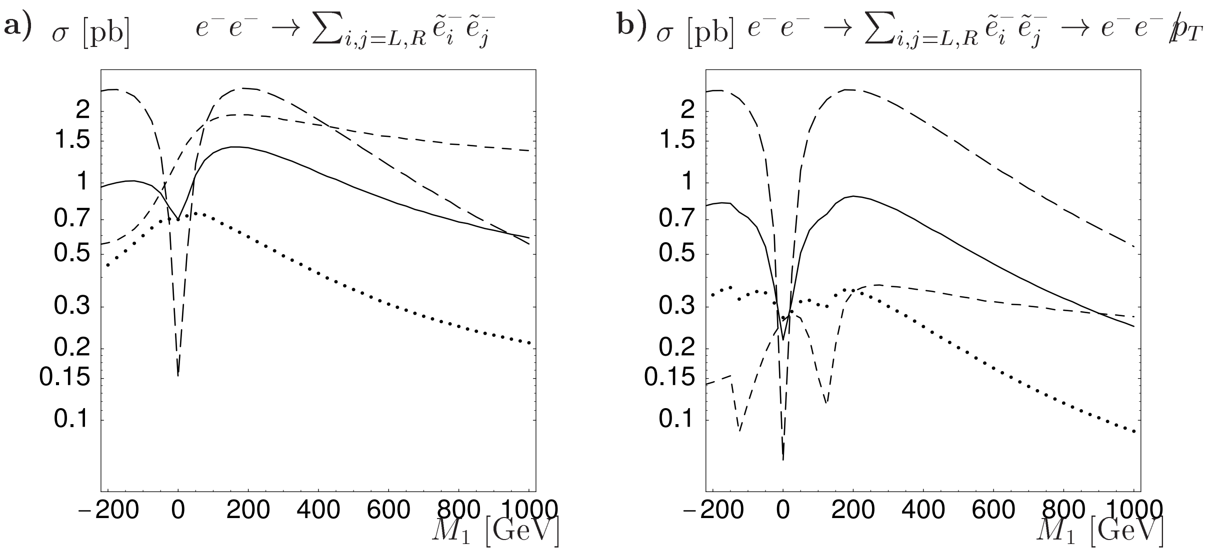

Figure 11: Cross sections for the processes $\sigma(e^-e^- \to \sum_{i,j=L,R} \tilde{e}_i^- \tilde{e}_j^-)$ (**a**) and $\sigma(e^-e^- \to \sum_{i,j=L,R} \tilde{e}_i^- \tilde{e}_j^- \to e^-e^- \not{p}_T)$ (**b**) as a function of M_1 for various polarizations. The effects of ISR- and beamstrahlung corrections are included. The graphs correspond to the following set of polarizations: full line $P_{e_1} = 0$, $P_{e_2} = 0$, dashed line $P_{e_1} = -0.8$, $P_{e_2} = -0.8$, dotted line $P_{e_1} = -0.8$, $P_{e_2} = 0.8$, and long dashed line $P_{e_1} = 0.8$, $P_{e_2} = 0.8$.

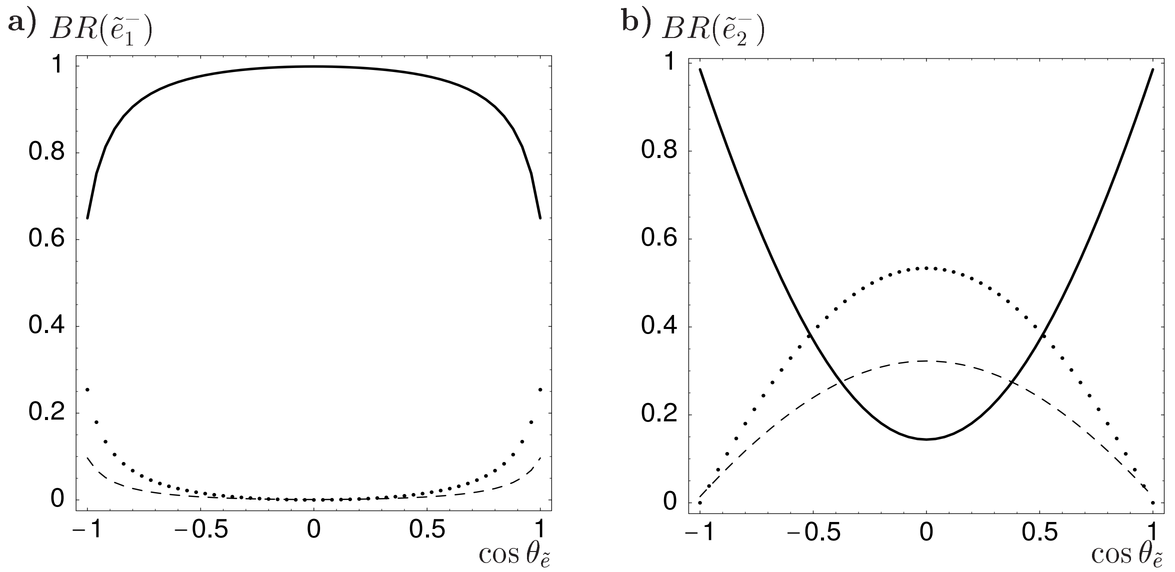

Figure 12: Branching ratios as a function of $\cos\theta_{\tilde{e}}$ for $\tilde{e}_1^-$ (**a**) and $\tilde{e}_2^-$ (**b**). Masses and gaugino parameters are as in scenario (I). The graphs correspond to: $BR(\tilde{e}_i^- \to e\tilde{\chi}_1^0)$ full line, $BR(\tilde{e}_i^- \to e\tilde{\chi}_2^0)$ dashed line, and $BR(\tilde{e}_i^- \to \nu_e\tilde{\chi}_1^-)$ dotted line.

matrix:

$$\mathcal{M}_{\tilde{e}}^2 = \begin{pmatrix} M_L^2 + v_1^2 h_e^2 + D_L & v_1 A_e - \mu h_e v_2 \\ v_1 A_e - \mu h_e v_2 & M_E^2 + v_1^2 h_e^2 + D_R \end{pmatrix} \tag{8}$$

with the D-terms $D_L = (-\frac{1}{2} + \sin^2\theta_W)\cos(2\beta)m_Z^2$ and $D_R = -\sin^2\theta_W \cos(2\beta)m_Z^2$. Here M_L^2, M_E^2, h_e, A_e, v_i are the left slepton mass parameter, the right slepton mass parameter, the lepton Yukawa coupling, the trilinear slepton–Higgs coupling and the vacuum expectation values, respectively. Motivated by supergravity theories it is usually assumed that $A_e = h_e \cdot O(100)$ GeV and in this case the off-diagonal element is negligible. However, this need not to be the case and it might be that $v_1 A_e$ is large enough to induce a sizable mixing between left- and right selectrons. In the following we use the convention $\tilde{e}_1 = \cos\theta_{\tilde{e}}\tilde{e}_L + \sin\theta_{\tilde{e}}\tilde{e}_R$ and $\tilde{e}_2 = -\sin\theta_{\tilde{e}}\tilde{e}_L + \cos\theta_{\tilde{e}}\tilde{e}_R$. Let us first study the dependence of the branching on $\cos\theta_{\tilde{e}}$ which is displayed in Fig. 12. Here we take $m_{\tilde{e}_1} = 137.7$ GeV, $m_{\tilde{e}_2} = 179.3$ GeV and the gaugino/higgsino parameters as in scenario (I). Note, that for $\cos\theta_{\tilde{e}} = 0$ we have exactly the configuration of scenario (I) whereas for $\cos\theta_{\tilde{e}} = \pm 1$ left and right selectrons would exchange the roles as it might happen for example in theories with extra D-terms at the unification scale [23].

In Fig. 12a) we display the branching ratios for the lighter selectron $\tilde{e}_1^-$ as a function of $\cos\theta_{\tilde{e}}$. It decays mainly into the lightest neutralino even for $|\cos\theta_{\tilde{e}}| = 1$ where it is a pure left-selectron. This is simply due to kinematics. Therefore, for $|\cos\theta_{\tilde{e}}| \lesssim 0.4$ it might be difficult to decide whether the selectrons mix or not if one looks only at the branching ratios of the lighter selectron. In case of the heavier selectron $\tilde{e}_2^-$ the situation is in general much clearer as can be seen in Fig. 12b) because the various decay channels have sufficient phase space. For $|\cos\theta_{\tilde{e}}| \lesssim 0.4 - 0.5$ the decay into the lighter chargino (dotted line) dominates followed by the decay into the wino-like neutralino $\tilde{\chi}_2^0$ (dashed line). For $|\cos\theta_{\tilde{e}}| \gtrsim 0.5$ the decay into the lighter neutralino $\tilde{\chi}_1^0$ dominates which is due to kinematics and due to the fact that the right-component of the selectron grows. Note that these features are quite insensitive to

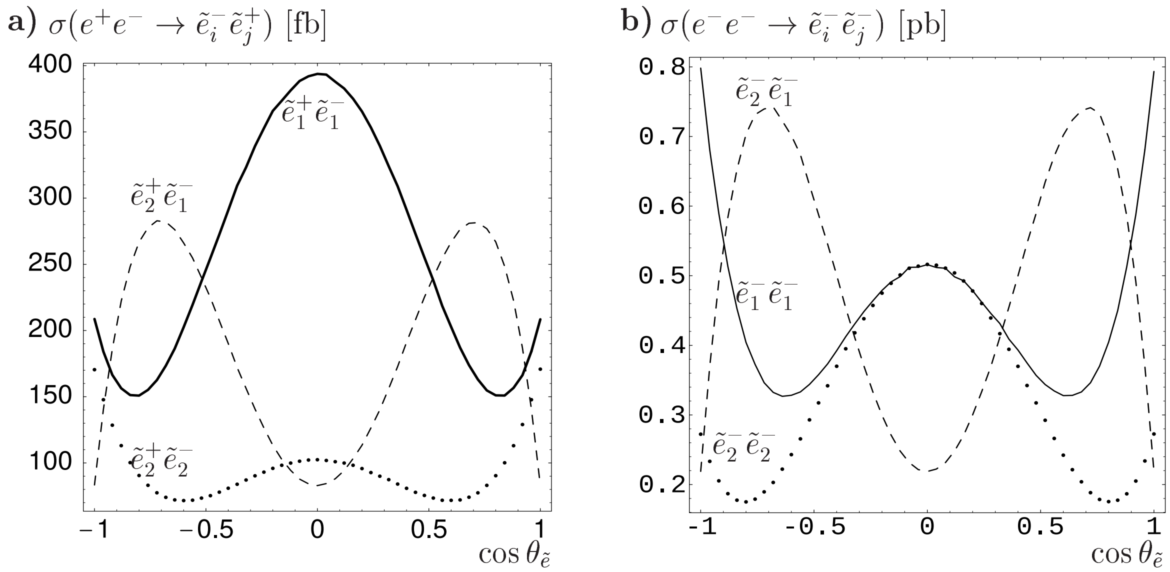

Figure 13: Production cross sections for selectrons as a function of $\cos\theta_{\tilde{e}}$ at (**a**) an e^+e^- collider and (**b**) an e^-e^- collider for $\sqrt{s} = 500$ GeV and unpolarized beams. ISR and beamstrahlung are included. We take the selectron masses and the gaugino/higgsino parameters as in scenario (I). The full line shows the cross section for pair production of the lighter selectrons, the dashed line a lighter and a heavier selectron, and the dotted line a pair of heavier selectrons.

$\tan\beta$ because even for $\tan\beta = 50$ the electron Yukawa coupling is still negligible (contrary to the case of staus as discussed e.g. in [24]).

In Fig. 13 we show the dependence of the cross sections on $\cos\theta_{\tilde{e}}$ for (**a**) an e^+e^- collider and (**b**) an e^-e^- collider at $\sqrt{s} = 500$ GeV with unpolarized beams. As can be seen there is a pronounced dependence on $\cos\theta_{\tilde{e}}$ at both collider types. Note that the production cross section for $\tilde{e}_1^- \tilde{e}_2^+$ is in general larger than that for the pair production in case of large mixing, $|\cos\theta_{\tilde{e}}| \simeq 1/\sqrt{2}$. Clearly the ratios of the various production channels are changed with varying beam polarization similarly as discussed in Sect. 2. As in the case of the decays the results for selectron production are quite insensitive to $\tan\beta$.

We have studied in Sect. 4 the possibility to test the weak quantum numbers L, R of the selectrons at an e^+e^- collider. We have shown that one can single out the $\tilde{e}_R^-\tilde{e}_L^+$ state depending on the polarization of the beams and one predicts a certain ratio of the various cross sections. In Fig. 13 one sees that there are several values of $\cos\theta_{\tilde{e}}$ with identical ratios of cross sections. Therefore the question arises whether it is possible to obtain the same polarization dependence of all cross sections for mixed selectrons as shown in Fig. 7 for the unmixed case. As can be seen in Fig. 14 the case $|\cos\theta_{\tilde{e}}| \lesssim 0.1$ might be difficult to distinguish from the unmixed case. However, for $0.2 \lesssim |\cos\theta_{\tilde{e}}| \lesssim 0.9$ it should be clear whether selectron mixing exists or not provided the neutralino sector is known so that one can calculate the cross sections.

7 Conclusion

In this paper we have studied selectron pair production in e^+e^- annihilation and in e^-e^- scattering with polarized electron and positron beams including ISR and beamstrahlung. We

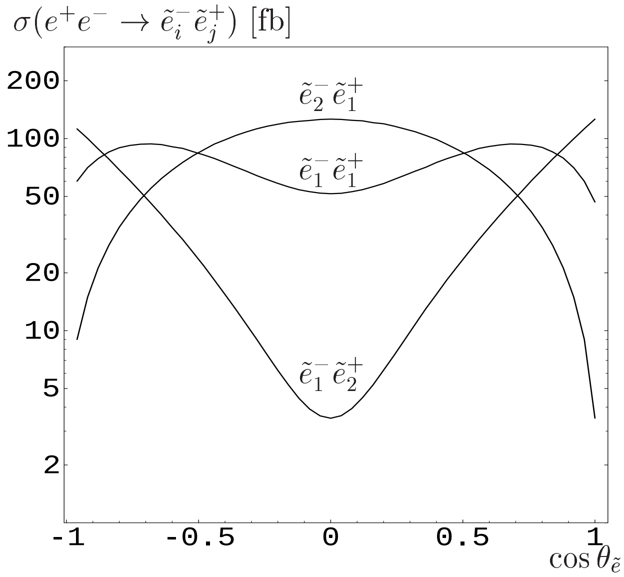

Figure 14: Production cross sections as a function of $\cos\theta_{\tilde{e}}$ for $\sqrt{s} = 350$ GeV, $P_{e^-} = -0.8$, $P_{e^+} = -0.6$, $m_{\tilde{e}_1} = 137.7$ GeV, $m_{\tilde{e}_2} = 179.3$ GeV and the other SUSY parameters as in scenario (I). ISR corrections and beamstrahlung are included.

have shown that at both collider modes all cross sections have a pronounced dependence on beam polarization. We have compared the possibility to measure the selectron masses using threshold scans at both colliders. Our results indicate that in the e^-e^- mode one tenth of the luminosity of the e^+e^- mode should be sufficient to obtain similar precision in the mass determination. Beam polarization is a useful tool to enhance the precision. Furthermore one can test the association between chiral electrons and their scalar superpartners at an e^+e^- collider if both beams are simultaneously polarized. We want to stress that in this case the polarization of the positron beam is indispensable. We also have studied the dependence of cross sections and branching ratios on the gaugino mass parameter M_1 which is pronounced at both colliders. In addition we have shown that the phenomenology of selectrons change significantly in case a non-vanishing mixing between left– and right–selectrons is realized in nature.

8 Acknowledgements

C.B. and W.P. thank M. Peskin for discussions on beamstrahlung. This work has been partly supported by the EU TMR Network Contract No. HPRN-CT-2000-00149. C.B. and H.F. are supported by the 'Deutsche Forschungsgemeinschaft' under contract number Fr 1064/5-1, W.P. is supported by 'Fonds zur Förderung der wissenschaftlichen Forschung' of Austria, Erwin Schrödinger fellowship Nr. J2095, and partly by the 'Schweizer Nationalfonds'.

A Lagrangian and couplings

In this section we list the lagrangian and the couplings for the calculation of selectron pair poduction. The selectron mass matrix in the most general form within the MSSM is given by:

$$\mathcal{M}^2_{\tilde{e}} = \begin{pmatrix} M_L^2 + v_1^2 h_e^2 + D_L & v_1 A_e - \mu h_e v_2 \\ v_1 A_e - \mu h_e v_2 & M_E^2 + v_1^2 h_e^2 + D_R \end{pmatrix} \tag{9}$$

with the D-terms $D_L = (-\frac{1}{2} + \sin^2\theta_W)\cos(2\beta)m_Z^2$ and $D_R = -\sin^2\theta_W \cos(2\beta)m_Z^2$. The mass eigenstates are connected via

$$\begin{pmatrix} \tilde{e}_1 \\ \tilde{e}_2 \end{pmatrix} = \begin{pmatrix} \cos\theta_{\tilde{e}} & \sin\theta_{\tilde{e}} \\ -\sin\theta_{\tilde{e}} & \cos\theta_{\tilde{e}} \end{pmatrix} \begin{pmatrix} \tilde{e}_L \\ \tilde{e}_R \end{pmatrix} \tag{10}$$

with the electroweak eigenstates and we take $m_{\tilde{e}_1} < m_{\tilde{e}_2}$.

The relevant parts of the interaction Lagrangian are given by:

$$\begin{aligned}
\mathcal{L}_{e\tilde{e}_k\tilde{\chi}^0_j} &= g f^L_j \bar{e}\left(a_{jk}P_R + b_{jk}P_L\right)\tilde{\chi}^0_j \tilde{e}_k + h.c. && (11)\\
\mathcal{L}_{\gamma\tilde{e}\tilde{e}} &= -ie_e A_\mu \left(\tilde{e}_1^* \overset{\leftrightarrow}{\partial_\mu} \tilde{e}_1 + \tilde{e}_2^* \overset{\leftrightarrow}{\partial_\mu} \tilde{e}_2\right) && (12)\\
\mathcal{L}_{Z\tilde{e}\tilde{e}} &= -igZ_\mu c_{ij} \tilde{e}_i^* \overset{\leftrightarrow}{\partial_\mu} \tilde{e}_j && (13)\\
\mathcal{L}_{\gamma ee} &= -e_e A_\mu \bar{e}\gamma^\mu e && (14)\\
\mathcal{L}_{Zee} &= -gZ_\mu \bar{e}\gamma^\mu (L_e P_L + R_e P_R)e && (15)
\end{aligned}$$

In the basis $\tilde{B}$, $\tilde{W}^3$, $\tilde{H}^0_d$, $\tilde{H}^0_u$, the couplings are given by

$$\begin{aligned}
a_{j1} &= \cos\theta_{\tilde{e}} f^L_j\,,\ a_{j2} = -\sin\theta_{\tilde{e}} f^L_j && (16)\\
b_{j1} &= \sin\theta_{\tilde{e}} f^R_j\,,\ b_{j2} = \cos\theta_{\tilde{e}} f^R_j && (17)\\
f^L_j &= \frac{1}{\sqrt{2}}\left(N_{j2} + \tan\theta_W N_{j1}\right) && (18)\\
f^R_j &= -\sqrt{2}\tan\theta_W N^*_{j1} && (19)\\
c_{11} &= R_e \sin^2\theta_{\tilde{e}} + L_e \cos^2\theta_{\tilde{e}} && (20)\\
c_{12} &= c_{21} = (L_e - R_e)\sin\theta_{\tilde{e}}\cos\theta_{\tilde{e}} && (21)\\
c_{22} &= L_e \sin^2\theta_{\tilde{e}} + R_e \cos^2\theta_{\tilde{e}} && (22)\\
L_e &= -\frac{1}{\cos\theta_W}\left(\frac{1}{2} - \sin^2\theta_W\right) && (23)\\
R_e &= \sin\theta_W \tan\theta_W && (24)
\end{aligned}$$

e_e is the electromagnetic coupling of the electron, respectively. We have neglected the electron Yukawa coupling. N_{ij} are the components of the neutralino mixing matrix.

B Amplitudes and cross section for selectron production in e^+e^- annihilation

We give the helicity amplitudes and cross section for the process $e^-(p_1, \lambda_m)e^+(p_2, \lambda_n) \to \tilde{e}_i^-(p_3)\tilde{e}_j^+(p_4)$, where λ_m (λ_n) denotes the helicity of e^- (e^+) and $i, j = 1, 2$.

The helicity amplitudes $T_{ij}^{\lambda_m\lambda_n}$ are:

$$\begin{aligned} T_{ij}^{\lambda_m\lambda_n}(\gamma) &= e^2\Delta(\gamma)\delta_{ij}\bar{v}(p_2,\lambda_n)(\not{p}_4-\not{p}_3)u(p_1,\lambda_m) \end{aligned} \tag{25}$$

$$\begin{aligned} T_{ij}^{\lambda_m\lambda_n}(Z) &= g^2 c_{ij}\Delta(Z) \\ &\quad \times\bar{v}(p_2,\lambda_n)(\not{p}_4-\not{p}_3)(L_\ell P_L+R_\ell P_R)u(p_1,\lambda_m) \end{aligned} \tag{26}$$

$$\begin{aligned} T_{ij}^{\lambda_m\lambda_n}(\tilde{\chi}^0_k) &= g^2\,\Delta(\tilde{\chi}^0_k)\,\bar{v}(p_2,\lambda_n)(a_{ki}P_R+b_{ki}P_L) \\ &\quad \times(\not{p}_1-\not{p}_3+m_{\tilde{\chi}^0_k})(a^*_{kj}P_L+b^*_{kj}P_R)u(p_1,\lambda_m) \end{aligned} \tag{27}$$

The propagators are:

$$\Delta(\gamma) = \frac{i}{(p_1+p_2)^2} \tag{28}$$

$$\Delta(Z) = \frac{i}{(p_1+p_2)^2-m_Z^2+im_Z\Gamma_Z} \tag{29}$$

$$\Delta(\tilde{\chi}^0_k) = \frac{i}{(p_1-p_3)^2-m^2_{\tilde{\chi}^0_k}} \tag{30}$$

The amplitudes squared are most easily expressed in terms of Mandelstam variables: $s=(p_1+p_2)^2=(p_3+p_4)^2$, $t=(p_1-p_3)^2=(p_2-p_4)^2$ and $u=(p_1-p_4)^2=(p_2-p_3)^2$. We further introduce four polarization factors:

$$c_{-+} = (1-P_{e^-})(1+P_{e^+}) \tag{31}$$

$$c_{+-} = (1+P_{e^-})(1-P_{e^+}) \tag{32}$$

$$c_{--} = (1-P_{e^-})(1-P_{e^+}) \tag{33}$$

$$c_{++} = (1+P_{e^-})(1+P_{e^+}) \tag{34}$$

where the first (second) index denotes the sign of the favoured helicity of e^- (e^+) and $P_{e^\pm}$ gives the corresponding polarization of $e^\pm$.

$$|T_{ij}(\gamma)|^2 = 4e_e^4\delta_{ij}|\Delta(\gamma)|^2(c_{-+}+c_{+-})(u\,t-m_i^2m_j^2) \tag{35}$$

$$T_{ij}(\gamma)T^*_{ij}(Z) = 4e_e^2g^2\delta_{ij}c_{ij}\Delta(\gamma)\Delta^*(Z)(c_{-+}L_e+c_{+-}R_e)(u\,t-m_i^2m_j^2) \tag{36}$$

$$\begin{aligned} T_{ij}(\gamma)T^*_{ij}(\tilde{\chi}^0_k) &= 2e_e^2g^2\delta_{ij}\Delta(\gamma)\Delta^*(\tilde{\chi}^0_k) \\ &\quad \times(c_{-+}|a_{ki}|^2+c_{+-}|b_{ki}|^2)(u\,t-m_i^2m_j^2) \end{aligned} \tag{37}$$

$$|T_{ij}(Z)|^2 = 4g^4c_{ij}^2|\Delta(Z)|^2(c_{-+}L_e^2+c_{+-}R_e^2)(u\,t-m_i^2m_j^2) \tag{38}$$

$$\begin{aligned} T_{ij}(Z)T^*_{ij}(\tilde{\chi}^0_k) &= 2g^4c_{ij}\Delta(Z)\Delta^*(\tilde{\chi}^0_k) \\ &\quad \times(c_{-+}a_{ki}a^*_{kj}L_e+c_{+-}b_{ki}b^*_{kj}R_e)(u\,t-m_i^2m_j^2) \end{aligned} \tag{39}$$

$$\begin{aligned} T_{ij}(\tilde{\chi}^0_k)T^*_{ij}(\tilde{\chi}^0_l) &= 2g^4\Delta(\tilde{\chi}^0_k)\Delta^*(\tilde{\chi}^0_l) \\ &\quad \times\Big[\left(c_{++}a_{li}a^*_{ki}b_{lj}b^*_{kj}+c_{--}a_{lj}a^*_{kj}b_{li}b^*_{ki}\right)m_km_ls \\ &\quad +\left(c_{-+}a_{li}a^*_{ki}a_{lj}a^*_{kj}+c_{+-}b_{lj}b^*_{kj}b_{li}b^*_{ki}\right) \\ &\quad \times(u\,t-m_i^2m_j^2)\Big] \end{aligned} \tag{40}$$

Note that the terms proportional to s gives rise to an β dependence of the cross section near the thresold whereas terms proportional to $u\,t - m_i^2 m_j^2$ gives rise to the β^3 dependence of the cross section near the thresold.

The total cross section is given by:

$$\sigma(e^+e^- \to \tilde{e}_i^- \tilde{e}_j^+) \;=\; \frac{1}{64\pi\, s} \int dt \Big| \sum_{x=\gamma, Z, \tilde{\chi}^0_k} T_{ij}(x) \Big|^2 . \tag{41}$$

In the center of mass system one can express the Madelstam variables in terms of the beam energy E and the angle θ between the electron and the selectron $\tilde{e}_i^-$: $s = 4E^2$, $t = (m_i^2 + m_j^2 - s + \cos\theta\kappa(s, m_i^2, m_j^2))/2$ and $u = (m_i^2 + m_j^2 - s - \cos\theta\kappa(s, m_i^2, m_j^2))/2$ with $\kappa(x,y,z) = \sqrt{(x-y-z)^2 - 4yz}$. From this follows $ut - m_i^2 m_j^2 = \sin^2\theta\ \times \kappa^2(s, m_i^2, m_j^2)$ indicating the P-wave nature of the respective terms.

C Amplitudes and cross section for selectron production in e^-e^- scattering

Here we give the helicity amplitudes and cross section for the process $e^-(p_1, \lambda_m) e^-(p_2, \lambda_n) \to \tilde{e}_i^-(p_3) \tilde{e}_j^-(p_4)$, where $\lambda_{m,n}$ denotes the helicity of the electrons and $i, j = 1, 2$.

The helicity amplitudes $T_{ij}^{\lambda_m \lambda_n}$ are given by:

$$\begin{aligned} T_{ij,t}^{\lambda_m \lambda_n}(\tilde{\chi}^0_k) &= g^2\, \Delta_t(\tilde{\chi}^0_k)\, \bar{v}(p_2, \lambda_n)(a^*_{ki} P_L + b^*_{ki} P_R) \\ &\quad \times (\not{p}_1 - \not{p}_3 + m_{\tilde{\chi}^0_k})(a^*_{kj} P_L + b^*_{kj} P_R) u(p_1, \lambda_m) \end{aligned} \tag{42}$$

$$\begin{aligned} T_{ij,u}^{\lambda_m \lambda_n}(\tilde{\chi}^0_k) &= g^2\, \Delta_u(\tilde{\chi}^0_k)\, \bar{v}(p_2, \lambda_n)(a^*_{kj} P_L + b^*_{kj} P_R) \\ &\quad \times (\not{p}_1 - \not{p}_4 + m_{\tilde{\chi}^0_k})(a^*_{ki} P_L + b^*_{ki} P_R) u(p_1, \lambda_m). \end{aligned} \tag{43}$$

The subscripts t and u indicate the t-channel and u-channel, respectively. The propagators are given by:

$$\Delta_t(\tilde{\chi}^0_k) \;=\; \frac{i}{(p_1 - p_3)^2 - m^2_{\tilde{\chi}^0_k}}, \tag{44}$$

$$\Delta_u(\tilde{\chi}^0_k) \;=\; \frac{i}{(p_1 - p_4)^2 - m^2_{\tilde{\chi}^0_k}}. \tag{45}$$

For the calculation of the amplitude squared we define the Mandelstam variables in the same terms of momenta as above. Similarly as above we define four polarization factors:

$$c_{-+} \;=\; (1 - P_{e_1})(1 + P_{e_2}) \tag{46}$$

$$c_{+-} \;=\; (1 + P_{e_1})(1 - P_{e_2}) \tag{47}$$

$$c_{--} \;=\; (1 - P_{e_1})(1 - P_{e_2}) \tag{48}$$

$$c_{++} \;=\; (1 + P_{e_1})(1 + P_{e_2}), \tag{49}$$

where the first (second) index denotes the sign of the favoured helicity of $e^-(p_1)$ $(e^-(p_2))$ and $P_{e_{1,2}}$ gives the corresponding polarization of $e^-(p_{1,2})$.

$$
\begin{aligned}
T_{ij,t}(\tilde{\chi}^0_k)T^*_{ij,t}(\tilde{\chi}^0_l) &= g^4\Delta_t(\tilde{\chi}^0_k)\Delta^*_t(\tilde{\chi}^0_l) \\
&\times\Big[\left(c_{+-}a_{li}a^*_{ki}b_{lj}b^*_{kj} + c_{-+}a_{lj}a^*_{kj}b_{li}b^*_{ki}\right)\left(t\,u - m_i^2m_j^2\right) \\
&+ \left(c_{++}b_{li}b^*_{ki}b_{lj}b^*_{kj} + c_{--}a_{li}a^*_{ki}a_{lj}a^*_{kj}\right)m_km_ls\Big] \qquad (50) \\
T_{ij,u}(\tilde{\chi}^0_k)T^*_{ij,u}(\tilde{\chi}^0_l) &= T_{ij,t}(\tilde{\chi}^0_k)T^*_{ij,t}(\tilde{\chi}^0_l)(i\leftrightarrow j, t\leftrightarrow u) \qquad (51) \\
T_{ij,t}(\tilde{\chi}^0_k)T^*_{ij,u}(\tilde{\chi}^0_l) &= g^4\Delta_t(\tilde{\chi}^0_k)\Delta^*_u(\tilde{\chi}^0_l) \\
&\times\Big[-\left(c_{-+}a_{lj}a^*_{kj}b_{li}b^*_{ki} + c_{+-}a_{li}a^*_{ki}b_{lj}b^*_{kj}\right)\left(t\,u - m_i^2m_j^2\right) \\
&+ \left(c_{--}a_{li}a^*_{ki}a_{lj}a^*_{kj} + c_{++}b_{li}b^*_{ki}b_{lj}b^*_{kj}\right)m_km_l\,s\Big] \qquad (52)
\end{aligned}
$$

The total cross section is given by:

$$
\begin{aligned}
\sigma(e^-e^-\to\tilde{e}^-_i\,\tilde{e}^-_j) &= \\
&\frac{1}{64\pi n!\,s}\int dt\left|\sum_{k=1}^{4}T_{ij,t}(\tilde{\chi}^0_k)+T_{ij,u}(\tilde{\chi}^0_k)\right|^2, \qquad (53)
\end{aligned}
$$

where n is the number of identical particles in the final state. The same consideration concering the center of mass system holds as in the case of e^+e^-.

References

[1] H. Murayama and M. E. Peskin, Ann. Rev. Nucl. Part. Sci. **46**, 533 (1996).

[2] E. Accomando *et al.*, ECFA/DESY LC Working Group, Phys. Rep. **299**, 1 (1998).

[3] J. A. Aguilar-Saavedra *et al.* [ECFA/DESY LC Physics Working Group Collaboration], hep-ph/0106315.

[4] G. Moortgat–Pick, H.M. Steiner, EPJdirect **C6**, (2001) 1.

[5] J.L. Feng, Int. J. Mod. Phys. **A 13** (1998) 2319.

[6] J. L. Feng and M. E. Peskin, Phys. Rev. D **64** (2001) 115002.

[7] U. Martyn, G. Blair, published in proceedings of 'Workshop on Linear Colliders (LCWS 99)', Sitges, Barcelona, Spain, 28 Apr - 5 May 1999, hep-ph/9910416; U. Martyn, Talk given at '5th International Linear Collider Workshop' (LCWS 2000), Fermilab, Batavia, Illinois, 24-28 Oct 2000, hep-ph/0002290.

[8] A. Bartl, H. Fraas, W. Majerotto, Z. Phys. **C 34**, 411 (1987); F. Cuypers, G. J. van Oldenborgh and R. Rückl, Nucl. Phys. B **409** (1993) 128; W. Y. Keung and L. Littenberg, Phys. Rev. D **28** (1983) 1067.

[9] G. Moortgat-Pick, A. Bartl, H. Fraas and W. Majerotto, Eur. Phys. J. C **18** (2000) 379; G. Moortgat-Pick, H. Fraas, A. Bartl and W. Majerotto, Eur. Phys. J. C **9** (1999) 521 [Erratum-ibid. C **9** (1999) 549].

[10] C. Blochinger and H. Fraas, published in '2nd ECFA/DESY Study 1998-2001', p. 632-641, hep-ph/0001034; C. Blöchinger, H. Fraas, T. Mayer and G. Moortgat-Pick, published in 'Batavia 2000, Physics and experiments with future linear e^+e^- colliders, AIP conference proceedings 578, p. 447-451, Eds. A. Para, H.E. Fisk, hep-ph/0101176; C. Blochinger, H. Fraas and T. Mayer, hep-ph/0109182.

[11] M. Skrzypek and S. Jadach, Z. Phys. C **49**, 577 (1991).

[12] M. E. Peskin, Linear Collider Collaboration technical note LCC–0010 (1999), http://www-sldnt.slac.stanford.edu/nlc/beamdeliveryhome.htm, and references therein.

[13] K. A. Thompson and P. Chen, SLAC-PUB-8230 *Presented at 4th International Workshop on Linear Colliders (LCWS 99), Sitges, Barcelona, Spain, 28 Apr - 5 May 1999.*

[14] H. Fraas, A. Freitas, G. Moortgat-Pick, W. Porod, in preparation.

[15] M. Dima *et al.*, hep-ex/0112017.

[16] A. Freitas, D.J. Miller, P.M. Zerwas, Eur. Phys. J. **C21**, 361 (2001).

[17] G. A. Blair, W. Porod and P. M. Zerwas, Phys. Rev. D **63** (2001) 017703.

[18] V. D. Barger, T. Han and R. J. Phillips, Phys. Rev. D **39** (1989) 146; A. Tofighi-Niaki and J. F. Gunion, Phys. Rev. D **39** (1989) 720.

[19] H. E. Haber and G. L. Kane, Phys. Rept. **117** (1985) 75.

[20] S. Y. Choi, J. Kalinowski, G. Moortgat-Pick and P. M. Zerwas, Eur. Phys. J. C **22** (2001) 563; S. Y. Choi, J. Kalinowski, G. Moortgat-Pick and P. M. Zerwas, DESY 02-020, hep-ph/0202039.

[21] U. Ellwanger, M. Rausch de Traubenberg and C. A. Savoy, Phys. Lett. B **315** (1993) 331; U. Ellwanger, M. Rausch de Traubenberg and C. A. Savoy, Nucl. Phys. B **492** (1997) 21; . Franke and H. Fraas, Int. J. Mod. Phys. A **12** (1997) 479; S. Hesselbach, F. Franke and H. Fraas, hep-ph/0107080.

[22] A. Masiero and J.W.F. Valle, Phys. Lett. B **251** (1990) 273; J.C. Romao, C.A. Santos and J.W.F. Valle, Phys. Lett. B **288** (1992) 311; G.F. Giudice, A. Masiero, M. Pietroni and A. Riotto, Nucl. Phys. B **396** (1993) 243; M. Shiraishi, I. Umemura and K. Yamamoto, Phys. Lett. B **313** (1993) 89.

[23] C. Kolda and S. P. Martin, Phys. Rev. D **53** (1996) 3871.

[24] A. Bartl, H. Eberl, S. Kraml, W. Majerotto and W. Porod, Z. Phys. C **73** (1997) 469; A. Bartl, H. Eberl, S. Kraml, W. Majerotto, W. Porod and A. Sopczak, Z. Phys. C **76** (1997) 549; A. Bartl, H. Eberl, S. Kraml, W. Majerotto and W. Porod, Eur. Phys. J. directC **6** (2000) 1.